Supporting Information

Regulation Effects of Co^{2+} in Constructing of Cu-$Ni(OH)_2$@CoO Nanoflower Clusters Heterojunction: A Critical Factor of Obtaining High-Performance Battery-type Hybrid Supercapacitor

Huifang Yang,[a] Haoran Guo,[a] Xinpan Li,[b] Wenlu Ren,[a] and Rui Song*[a]

[a]School of Chemical Sciences, University of Chinese Academy of Sciences, 19 Yuquan Road, Shijingshan District, Beijing, 100049, PR China

[b]Institute of Chemistry, Chinese Academy of Sciences (CAS), 2 Zhongguancun North Road, Haidian District, Beijing, 100190, PR China

E-mail: rsong@ucas.ac.cn

Experimental section

Pre-treatment of Ni-foam： First, several nickel foams (3 cm × 4 cm) were put in 6 M HCl solutions for 10 min to eliminate the surface oxides. Then, they were transferred into 20 mL acetone for 10 min to experience a process of degreasing. Finally, after 30 min ultrasonic cleaning and washing by deionized water, the nickel foams was taken to an oven with 60 ℃ for 1 h.

Preparation of Cu-Ni(OH)$_2$@CoO NFCs electrodes： The Cu-Ni(OH)$_2$@CoO NFCs composite is synthesized by a two-step hydrothermal method. In the first hydrothermal process, 0.3 g cupric sulfate ($CuSO_4 \cdot 5H_2O$) and 2 g urea were added into 30 mL deionized water under stirring to form a homogeneous and transparent solution. The precursors were made by immersing nickel foams in aqueous solution and transferred to a Teflon-lined stainless steel autoclave, then kept at 120 ℃ for 6 h. In the second steps, after washed by deionized water several times, the obtained electrode material is transferred to a Teflon-lined stainless steel autoclave which contains 30 ml of cobaltous nitrate hexahydrate ($Co(NO_3)_2 \cdot 6H_2O$, 0.3g) aqueous solution, then kept at 100 ℃ for 6 h. Ultimately, the synthetized sample was washed by deionized water several times and then transferred into an oven maintained at 60 ℃ overnight.

Assembly of flexible all-solid Hybrid Asymmetric Supercapacitors： 6 g polyvinyl alcohol (PVA) and 3 g KOH were added into 60 mL deionized water to prepare gel electrolytes for HASC. First, the above solution is heated to 100 ℃ for 30 min to obtain a homogeneous solution, then the positive electrode materials (Cu-

$Ni(OH)_2$@CoO NFCs, 1 cm^2) and negative electrode materials (porous carbon coated nickel foam, 1 cm^2) were immersed into the PVA/KOH electrolytes for 1 min. After repeated soaking for three times, the electrodes were transferred to a petri dish and stand for 12 h before being assembled into a flexible all-solid HASC. And the specific assembly procedures of flexible all-solid HASC could be found in our previous work.[1]

Characterization methods

A Rigaku Smartlab X-ray diffraction (XRD) equipment was applied to collect the diffraction data of the obtained samples using Cu Kα (λ = 0.1544 nm) radiation. Moreover, a Renishaw Invia Raman spectrometer with a 20 mW Ar^+ laser source of 532 nm was used to collect the Raman spectra. The morphologies and structures of samples were investigated by a field emission scanning electron microscope (FESEM) (Regulus 8220). In addition, a transmission electron microscopy (TEM, Tecnai F30, S-TWIN) coupled with an energy-dispersive X-ray spectroscopy (EDS) were conducted to detect the microstructure of active materials. The X-ray photoelectron spectra (XPS) were also measured on a Thermo Scientific ECSALab 250Xi X-ray photoelectron spectrometer with an Al Kα X-ray radiation (1486 eV) to investigate the chemical states and surface composition.

Electrochemical measurements

Evaluation of Supercapacitive Performances: All electrochemical tests were based on a CHI 660E electrochemical workstation (CH Instrumental Co, Ltd, Shanghai), and the electrochemical property of individual electrode is studied by a three-electrode electrochemical set-up (Pt foil as the counter electrode, saturated calomel electrode (SCE) as the reference electrode and the self-supported Cu-$Ni(OH)_2$@CoO NFCs as the working electrode, respectively). In this system, an aqueous solution of 3 M KOH was used as electrolyte, and the stability of electrode

was tested under the scan rate of 50 mV s^{-1}. Besides, the range of frequency in the electrochemical impedance spectroscopy (EIS) measurement is from 0.01 HZ to 100 KHz. Meanwhile, the galvanostatic charge-discharge (GCD) tests were carried out from -0.1 V to 0.4 V and the areal specific capacitance (C_s) were calculated by the equation as follows:

$$C_s = It / A\Delta V \tag{1}$$

Where C_s is the areal specific capacitance (mF·cm^{-2}), I is the discharge current (A), t is the discharge time (s), A represents the area of self-supported electrodes (cm^2) and △V is the potential window (V).

Besides, the energy density and power density of $Ni(OH)_2$@CoO NFCs//porous carbon HASC are calculated by the two equations as follows:

$$E = {}^{1}/_{2} C_s V^2 \tag{2}$$

$$P = E/t \tag{3}$$

Where E represents the energy density (mWh·cm^{-2}), C_s is the areal specific capacitance (F·cm^{-2}), V means the operating voltage (V), P is the power energy (mW·cm^{-2}), t refers to the discharge time (s).

Also, to achieve $q_+ = q_-$, the mass ratio of positive electrode active material to negative electrode active material is determined from the following equation:

$$m_+ : m_- = \left(\int \frac{idV}{v}\right)_- : \left(\int \frac{idV}{v}\right)_+ \tag{4}$$

The mass ratio of the positive electrode active material to the negative electrode active materials was determined from the cyclic voltammetry acquired at 10mV/s for both electrodes.

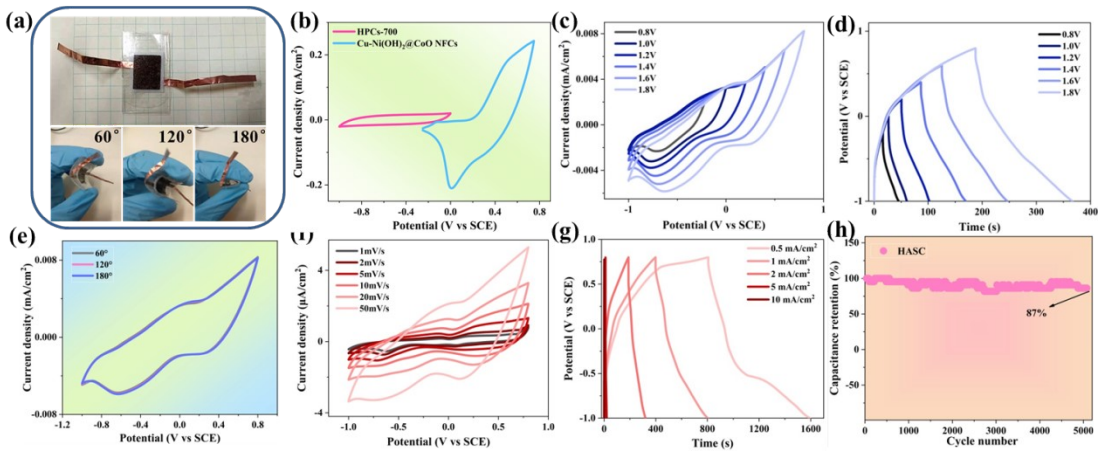

Figure S1. (**a**) The photo of obtained flexible all-solid supercapacitor device with different bend angles; (**b**) CV curves of Cu-Ni(OH)$_2$@CoO NFCs and porous carbon at a scan rate of 100 mV·s^{-1} in a three-electrode system; (**c**) CV plots of Cu-Ni(OH)$_2$@CoO NFCs//porous carbon HASC at different potential windows; (**d**) GCD curves of Cu-Ni(OH)$_2$@CoO NFCs//porous carbon HASC at different potential windows from 0.8 to 1.8 V; (**e**) CV plots of Cu-Ni(OH)$_2$@CoO NFCs//porous carbon HASC at different bend angles; (**f**) CV plots of Cu-Ni(OH)$_2$@CoO NFCs//porous carbon HASC at various scan rates; (**g**) GCD plots of Cu-Ni(OH)$_2$@CoO NFCs//porous carbon HASC at various current density; (**h**) a function of specific capacitance of Cu-Ni(OH)$_2$@CoO NFCs//porous carbon HASC to current density.

A flexible solid-state HASC was fabricated to explore the practical application of electrode materials. In the assemble procedure, the as-prepared Cu-Ni(OH)$_2$@CoO NFCs, porous carbon from our previous work[1] and PVA/KOH gel were chosen as positive electrode, negative electrode and electrolyte, respectively. The outstanding flexibility of assembled HASC device is displayed in the **Figure. S1a**, and the shape of CV plots at different bend angles (**Figure. S1e**) is nearly unchanged at all. As shown in **Figure. S1b**, the potential windows of Cu-Ni(OH)$_2$@CoO NFCs//porous carbon HASC

were determined through the test of voltage range at a scan rate of 100 mV s^{-1}. As depicted in **Figure. S1c** and **S1d**, the CV and GCD tests were conducted at different potential windows from 0.8 V to 1.8 V. No obvious polarization could be observed when the potential window was less than 1.8 V (**Figure. S1c**), suggesting that the operating voltage of HASC could be broadened up to 1.8 V. As displayed in **Figure. S1f**, a series of redox peaks appeared at the CV plots in different scan rates, indicating that both pseudo-capacitance and double-layer capacitance take effect in the process of electrode reactions.[2] Furthermore, the CV curves of HASC device nearly remain its initial shape, suggesting a good reversibility.[3] Additionally, based on **Figure. S1g** and **Equation 1**, the mass loading of the positive and negative electrode in the assembled HASC are 0.0022 g and 0.0153 g, and the areal specific capacitances of Cu-$Ni(OH)_2$@CoO NFCs//porous carbon HASC can be calculated to be 996.6 mF cm^{-2} at current density of 1.0 mA cm^{-2}.

Energy density and power density are two important parameters in evaluating supercapacitive performance. The obtained Cu-$Ni(OH)_2$@CoO NFCs//porous carbon HASC device exhibits a superior energy density of 0.45 mWh cm^{-2} when its power energy up to 9 mW cm^{-2}, exceeding most of transition-metal based asymmetric supercapacitors. The comparatively detailed parameters with some recent publications can be found in the *Ragone* plots (**Figure. S9)** and **Table S4**. Furthermore, the values of R_s and R_{ct} derived from the EIS measurement in **Figure. S8** are treated as the criterion of evaluating the charge transfer process, which demonstrates a superior electrochemistry property for Cu-$Ni(OH)_2$@CoO NFCs//porous carbon HASC.[4] In

addition, the durability of HASC was explored through charge and discharge cycle test at a current density of 1 mA cm^{-2}. No abnormal fluctuations are witnessed during testing, and the capacitance still remains *ca*.87% after 5000 cycles (**Figure. S1h**). Besides, the coulombic efficiency of HASC can reach to 92.4%, indicating an excellent reversibility (**Figure. S10**).[5] To sum up, the Cu-$Ni(OH)_2$@CoO NFCs//porous carbon flexible solid-state HASC device displays an admirable performance.

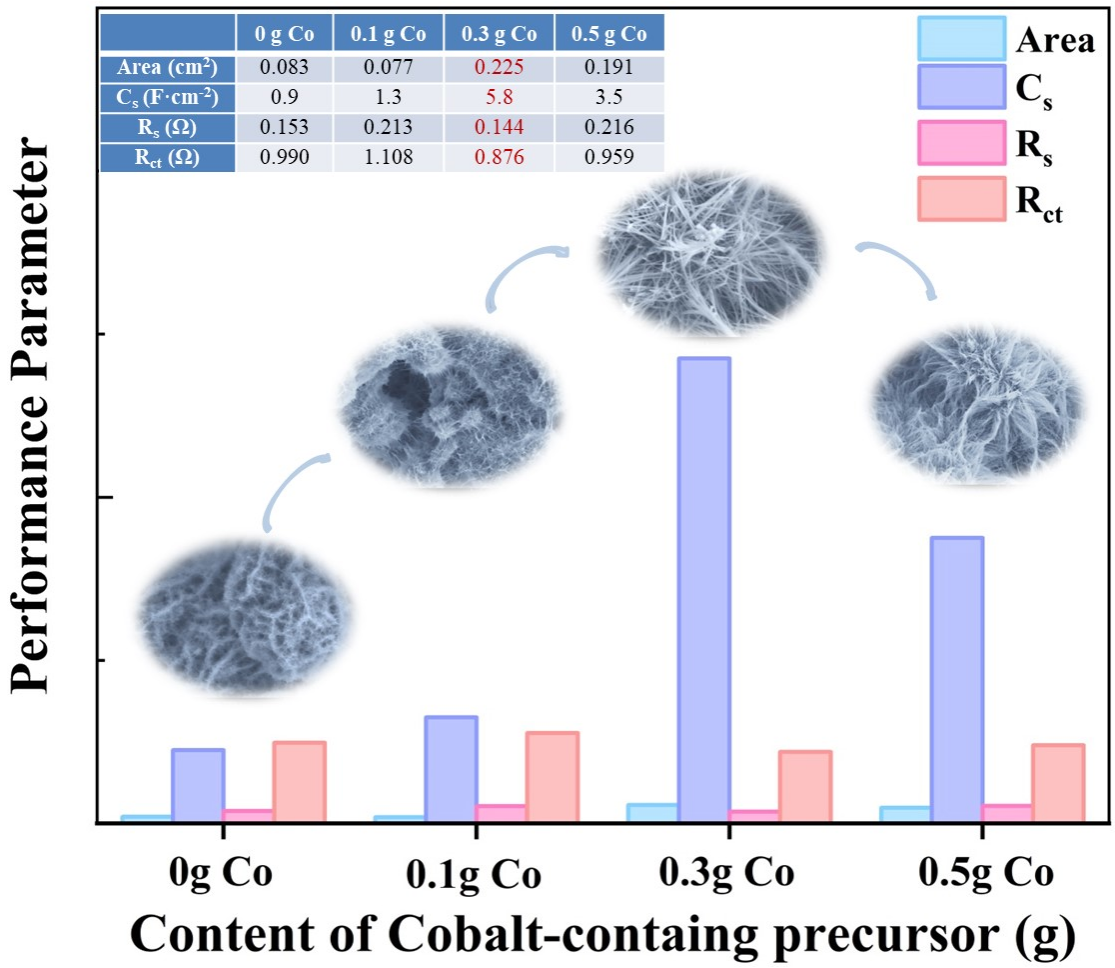

Figure S2. Relationship between properties parameters (Area: the area of one CV cycle; C_s: areal specific capacitance of electrode materials; R_s: the equivalent series resistance; R_{ct}: charge transfer resistance) and content of precursor Co-containing.

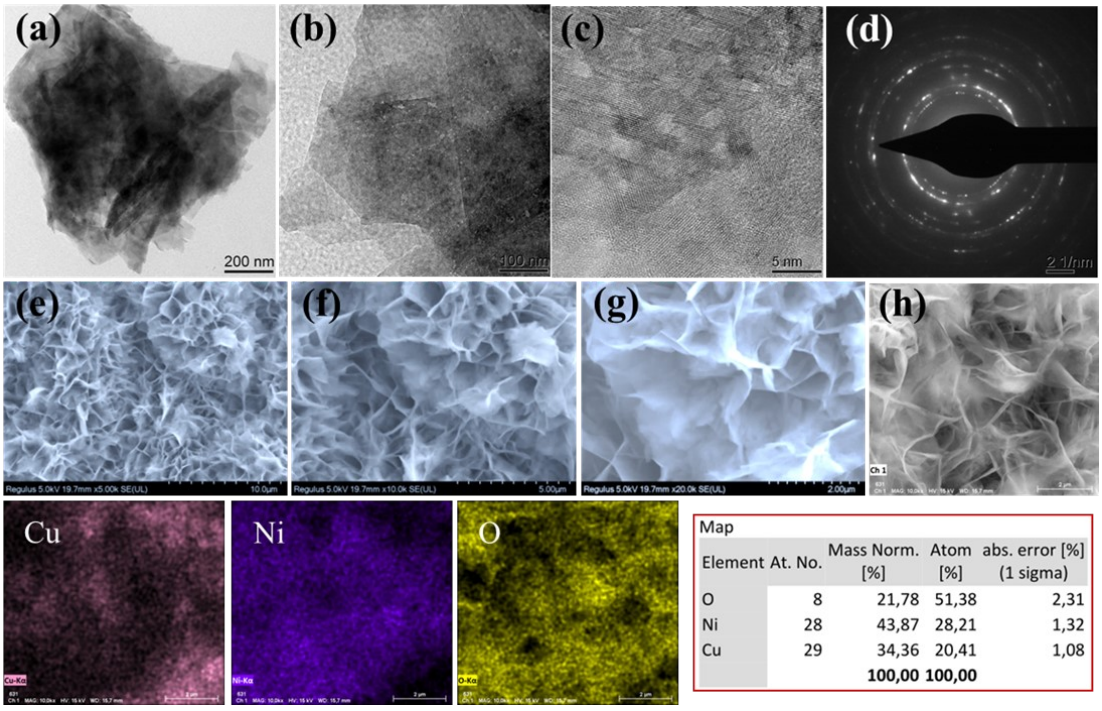

Map

Element	At. No.	Mass Norm. [%]	Atom [%]	abs. error [%] (1 sigma)
O	8	21,78	51,38	2,31
Ni	28	43,87	28,21	1,32
Cu	29	34,36	20,41	1,08
		100,00	**100,00**	

Figure S3. TEM images (**a-d**); SEM images (**e-g**) and EDS analyses (**h**) of typical Cu-$Ni(OH)_2$ NAs active materials with different magnifications and locations of sample.

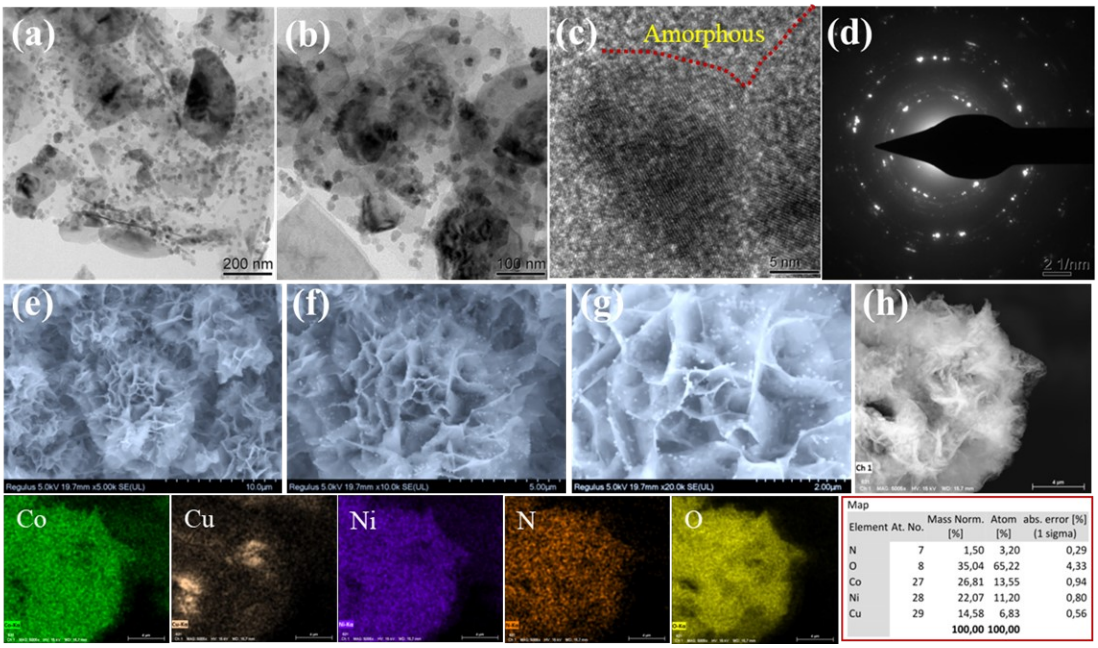

Figure S4. TEM images (**a-d**); SEM images (**e-g**) and EDS analyses (**h**) of typical Cu-$Ni(OH)_2$@CoO NAs; active materials with different magnifications and locations of sample.

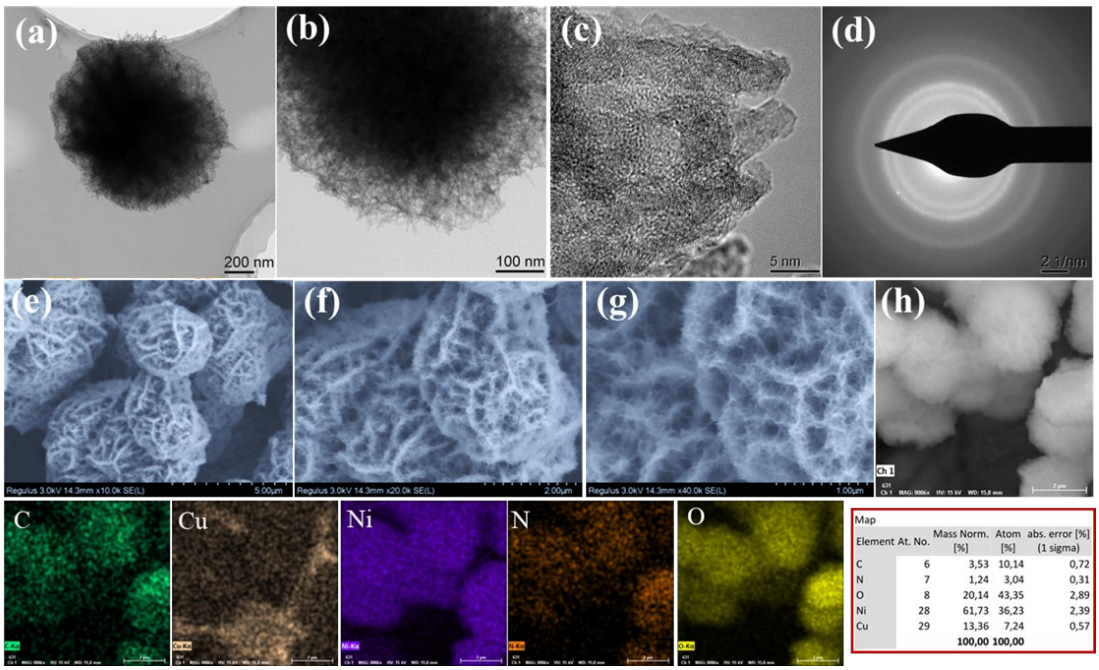

Figure S5. TEM images (**a-d**); SEM images (**e-g**) and EDS analyses (**h**) of typical Cu-$Ni(OH)_2$ NBs active materials with different magnifications and locations of sample.

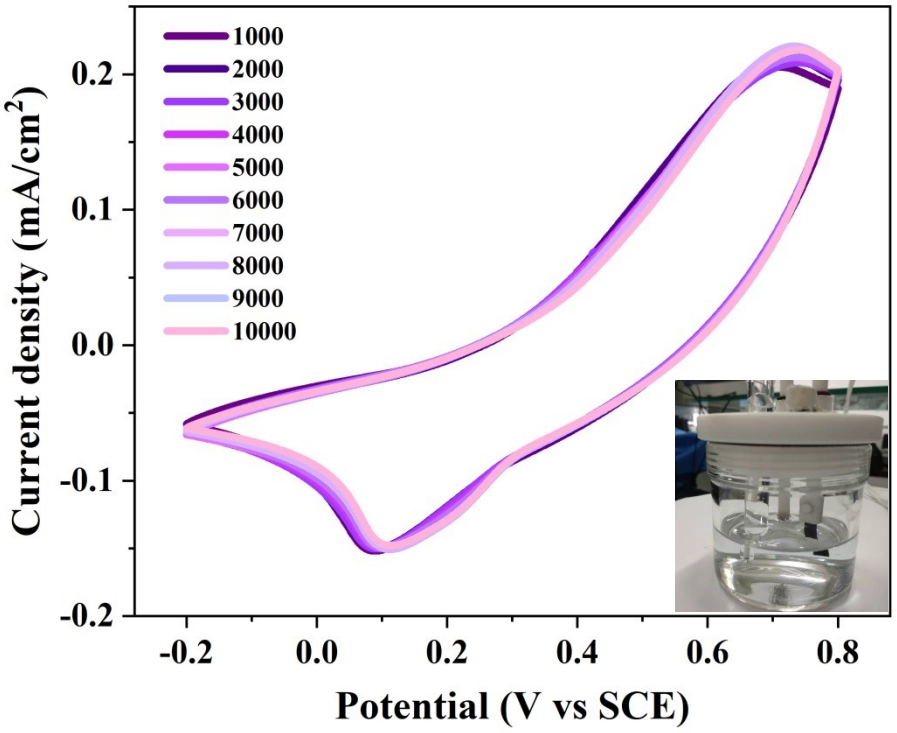

Figure S6. Comparison of CV curves at different cycle numbers for Cu-Ni(OH)$_2$@CoO NFCs electrode.

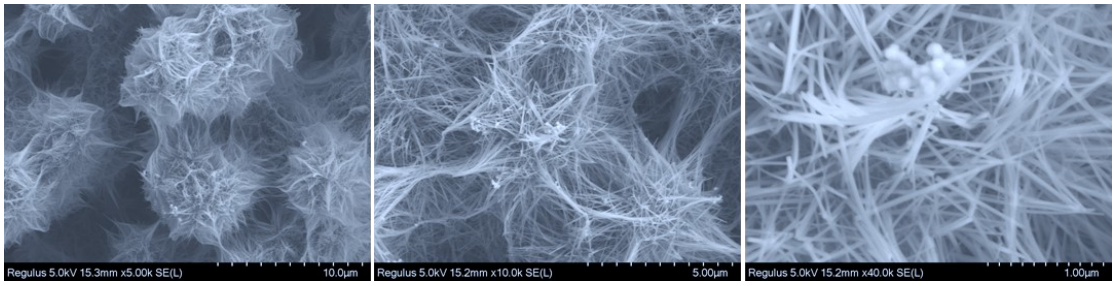

Figure S7. SEM images of Cu-Ni$(OH)_2$@CoO NFCs after 10000 CV cycles.

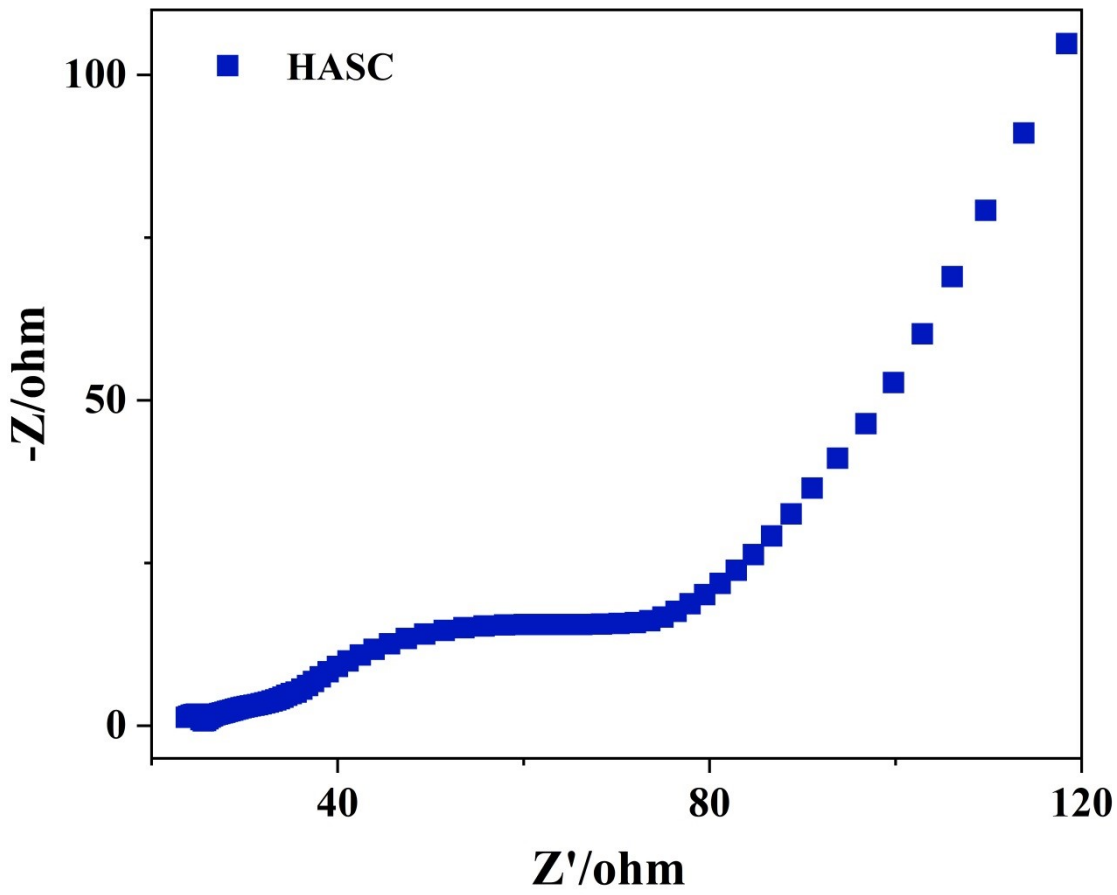

Figure S8. Nyquist plots of Cu-Ni$(OH)_2$@CoO NFCs//porous carbon HASC.

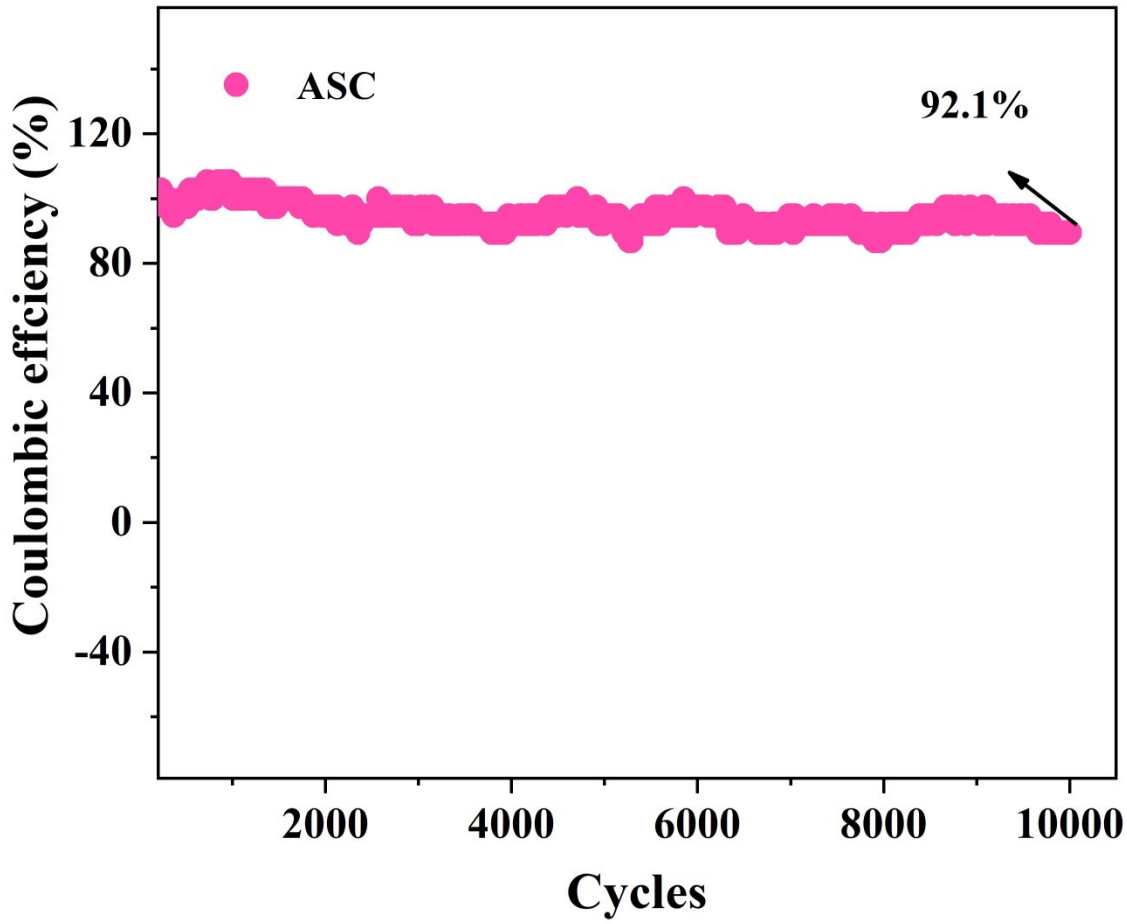

Figure S9. Coulomb efficiency of Cu-Ni$(OH)_2$@CoO NFCs//porous carbon HASC as a function of cycle number.

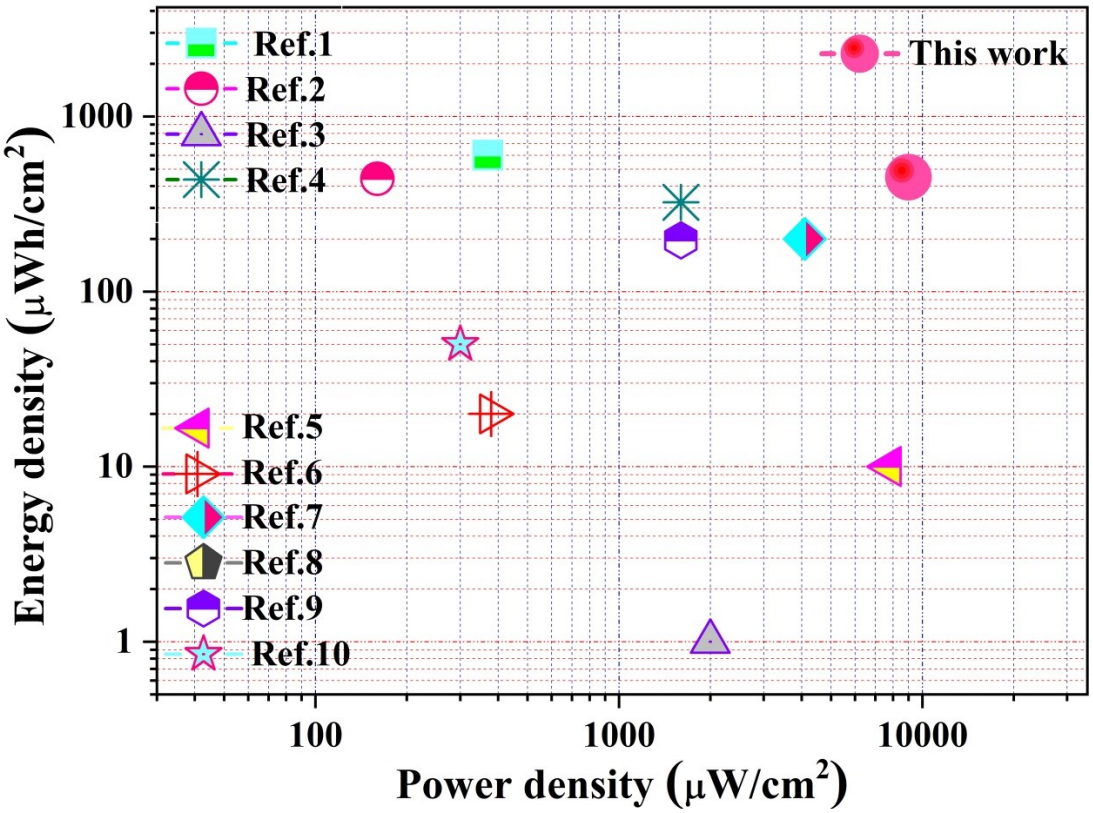

Figure S10. *Ragone* plots showing the comparison of Cu-Ni$(OH)_2$@CoO NFCs//porous carbon HASC with other Ni/Co-based devices.

Table S1. Comparison of several electrode materials in the terms of conductivity

	Resistivity **(μΩ·m)**	***Conductivity*** **(S/m)**
Cu-Ni(OH)$_2$ NAs	3.98313	251059.08401
Cu-Ni(OH)$_2$@CoO NAs	5.10301	195962.92514
Cu-Ni(OH)$_2$ NBs	4.42779	225846.52941
Cu-Ni(OH)$_2$@CoO NFCs	3.17578	314883.03737

Table S2. The values of R_s and R_{ct} for Cu-Ni(OH)$_2$ NAs, Cu-Ni(OH)$_2$@CoO NAs, Cu-Ni(OH)$_2$ NBs and Cu-Ni(OH)$_2$@CoO NFCs electrodes

	Cu-Ni(OH)$_2$ NAs	**Cu-Ni(OH)$_2$@CoO NAs**	**Cu-Ni(OH)$_2$ NBs**	**Cu-Ni(OH)$_2$@CoO NFCs**
R_s (Ω)	0.142	0.162	0.158	0.131
R_{ct} (Ω)	1.132	1.035	1.125	1.023

Table S3. Comparison of Ni/Co-based materials applied to supercapacitors

Electrode	Electrolyte	Areal specific capacitance	current density	Reference
Ni/Co-oxyhydroxides	6 M KOH	8.87 $F \cdot cm^{-2}$	5 $mA \cdot cm^{-2}$	[6]
CoO@Ni(OH)$_2$ core–shell	2 M KOH	1418.2 $F \cdot g^{-1}$	1 $A \cdot g^{-1}$	[7]
Ni(OH)$_2$/CoO/rGO	3 M KOH	1056 $F \cdot g^{-1}$	5 $mV \cdot s^{-1}$	[8]
VCO/CNFs	1 M KOH	1.83 $F \cdot cm^{-2}$	8 $mA \cdot cm^{-2}$	[9]
CoO@CoS/Ni$_3$S$_2$	2 M KOH	2506 $F \cdot g^{-1}$	1 $A \cdot g^{-1}$	[10]
CoO-GHBs/CC	5 M KOH	2238 $F \cdot g^{-1}$	1 $A \cdot g^{-1}$	[11]
CoO/NiO−Cu@CuO	6 M KOH	2.03 $F \cdot cm^{-2}$	2 $mA \cdot cm^{-2}$	[12]
CoO/Co-Cu-S	2 M KOH	2300 $F \cdot g^{-1}$	2 $A \cdot g^{-1}$	[13]
CuCoO-H	3 M KOH	405.36 $F \cdot g^{-1}$	20 $A \cdot g^{-1}$	[14]
Cu-Ni(OH)$_2$@CoO NFCs	**3 M KOH**	**5.8 $F \cdot cm^{-2}$**	**1 $mA \cdot cm^{-2}$**	**This work**

Table S4. Comparison of Ni/Co-based materials assembled to HASC in the field of supercapacitors

HASC	C_s (mF cm^{-2})	E (mWh cm^{-2})	P (mW cm^{-2})	Reference
Ni@Ni(OH)$_2$/ACC	**1910**	**0.6**	**0.37**	[15]
Ni$_2$CoS$_4$@NiCo$_2$O$_4$/CFP	**1250**	**0.44**	**0.16**	[16]
NiCo$_2$O$_4$ NG @ CF	**25**	**0.001**	**2**	[17]
PNH@NeC LDH//AC	**21**	**0.323**	**1.6**	[18]
NiO/Ni(OH)$_2$/ PEDOT//AC	**404**	**0.01**	**7.8**	[19]
NiO@MnCo-LDH//Ni/AC	**368**	**0.02**	**0.38**	[20]
3D-NiMoO$_4$/Ni@CW//rGO/CF	**504**	**0.2**	**4.1**	[21]
Co(OH)$_2$@Ni/Ag-mesh	**248**	**0.00042**	**0.00833**	[22]
blanket-like Co(OH)$_2$/CoOOH/Co$_3$O$_4$/Cu(OH)$_2$	**888**	**0.196**	**1.6**	[23]
NiO//α-Fe$_2$O$_3$	**229**	**0.05**	**0.3**	[24]
Cu-Ni(OH)$_2$@CoO NFCs//Porous carbon	**996.6**	**0.45**	**9.0**	**This work**

References

(1) Fan, P.; Ren, J.; Pang, K.; Cheng, Y.; Wu, X.; Zhang, Z.; Ren, J.; Huang, W.; Song, R., Cellulose-Solvent-Assisted, One-Step Pyrolysis to Fabricate Heteroatoms-Doped Porous Carbons for Electrode Materials of Supercapacitors. *ACS Sustainable Chemistry & Engineering* **2018,** *6* (6), 7715-7724.

(2) Zardkhoshoui, A. M.; Davarani, S. S. H., Construction of complex copper-cobalt selenide hollow structures as an attractive battery-type electrode material for hybrid supercapacitors. *Chemical Engineering Journal* **2020,** *402*, 126241.

(3) Fu, M.; Lv, R.; Lei, Y.; Terrones, M., Ultralight Flexible Electrodes of Nitrogen-Doped Carbon Macrotube Sponges for High-Performance Supercapacitors. *Small* **2021,** *17* (1), e2004827.

(4) Chen, F.; Chen, C.; Hu, Q.; Xiang, B.; Song, T.; Zou, X.; Li, W.; Xiong, B.; Deng, M., Synthesis of CuO@CoNi LDH on Cu foam for high-performance supercapacitors. *Chemical Engineering Journal* **2020,** *401*, 126145.

(5) Wang, Y.; Wang, X.; Li, X.; Li, X.; Liu, Y.; Bai, Y.; Xiao, H.; Yuan, G., A High-Performance, Tailorable, Wearable, and Foldable Solid-State Supercapacitor Enabled by Arranging Pseudocapacitive Groups and MXene Flakes on Textile Electrode Surface. *Advanced Functional Materials* **2020,** *31* (7), 2008185.

(6) Pan, M.; Zeng, W.; Quan, H.; Cui, J.; Guo, Y.; Wang, Y.; Chen, D., Low-crystalline Ni/Co-oxyhydroxides nanoarrays on carbon cloth with high mass loading and hierarchical structure as cathode for supercapacitors. *Electrochimica Acta* **2020**, 357, 136886.

(7) Wu, W.; Xia, P.; Xuan, Y.; Yang, R.; Chen, M.; Jiang, D., Hierarchical CoO@$Ni(OH)_2$ core-shell heterostructure arrays for advanced asymmetric supercapacitors. *Nanotechnology* **2020**, 31 (40), 405705.

(8) Jiang, L.; Zou, R.; Li, W.; Sun, J.; Hu, X.; Xue, Y.; He, G.; Hu, J., $Ni(OH)_2$/CoO/reduced graphene oxide composites with excellent electrochemical properties. *J. Mater. Chem. A* **2013**, 1 (3), 478-481.

(9) Nie, G.; Zhao, X.; Jiang, J.; Luan, Y.; Shi, J.; Liu, J.; Kou, Z.; Wang, J.; Long, Y.-Z., Flexible supercapacitor of high areal performance with vanadium/cobalt oxides on carbon nanofibers as a binder-free membrane electrode. *Chemical Engineering Journal* **2020**, 402, 126294.

(10) Zhang, Y.; Wang, D.; Lü, S.; Chen, Y.; Fan, H.; Wei, M.; Yang, L.; Yu, W. W.; Meng, X., CoO@CoS/Ni_3S_2 hierarchical nanostructure arrays for high performance asymmetric supercapacitor. *Applied Surface Science* **2020**, 532, 147438.

(11) Tseng, C. A.; Sahoo, P. K.; Lee, C. P.; Lin, Y. T.; Xu, J. H.; Chen, Y. T., Synthesis of CoO-Decorated Graphene Hollow Nanoballs for High-Performance Flexible Supercapacitors. *ACS Appl Mater Interfaces* **2020**, 12 (36), 40426-40432.

(12) Zhang, A.; Yue, L.; Jia, D.; Cui, L.; Wei, D.; Huang, W.; Liu, R.; Liu, Y.; Yang, W.; Liu, J., Cobalt/Nickel Ions-Assisted Synthesis of Laminated CuO Nanospheres Based on $Cu(OH)_2$ Nanorod Arrays for High-Performance Supercapacitors. *ACS Appl*

Mater Interfaces **2020**, 12 (2), 2591-2600.
(13) Lu, W.; Shen, J.; Zhang, P.; Zhong, Y.; Hu, Y.; Lou, X. W. D., Construction of CoO/Co-Cu-S Hierarchical Tubular Heterostructures for Hybrid Supercapacitors. *Angew Chem Int Ed Engl* **2019**, 58 (43), 15441-15447.
(14) Jin, C.; Cui, Y.; Zhang, G.; Luo, W.; Liu, Y.; Sun, Y.; Tian, Z.; Zheng, W., Synthesis of copper-cobalt hybrid oxide microflowers as electrode material for supercapacitors. *Chemical Engineering Journal* **2018**, 343, 331-339.
(15) Jin, Z.; Zhou, M.; Hu, J.; Li, K.; Tang, L.; Zhao, H.; Cai, Z.; Zhao, Y. J., Hierarchical Ni@$Ni(OH)_2$ core-shell hybrid arrays on cotton cloth fabricated by a top-down approach for high-performance flexible asymmetric supercapacitors. *Alloys Compd.* **2019**, 784, 1091-1098.
(16) Cao, L.; Tang, G.; Mei, J.; Liu, H., Construct hierarchical electrode with $Ni_xCo_{3-x}S_4$ nanosheet coated on $NiCo_2O_4$ nanowire arrays grown on carbon fiber paper for high-performance asymmetric supercapacitors. *J. Power Sources.* **2017**, 359, 262-269.
(17) Senthilkumar, S. T.; Fu, N.; Liu, Y.; Wang, Y.; Zhou, L.; Huang, H., Flexible fiber hybrid supercapacitor with $NiCo_2O_4$ nanograss@carbon fiber and bio-waste derived high surface area porous carbon. *Electrochim. Acta.* **2016**, 211, 411-419.
(18) Li, K.; Liu, M.; Li, S.; Huang, F.; Wang, L.; Zhang, H., Design on hierarchical P doped $Ni(OH)_2$@Ni-Co LDH core-shell heterojunction as an advanced battery-like electrode for high performance hybrid supercapacitors. *Journal of Alloys and Compounds* **2020**, 817, 152712.
(19) Yang, H.; Xu, H.; Li, M.; Zhang, L.; Huang, Y.; Hu, X., Assembly of NiO/$Ni(OH)_2$/PEDOT Nanocomposites on Contra Wires for Fiber-Shaped Flexible Asymmetric Supercapacitors. *ACS Appl. Mater. Interfaces.*, **2016**, 8, 1774-1779.
(20) Gao, L.; Fan, R.; Xiao, R.; Cao, K.; Li, P.; Wang, W.; Lu, Y., NiO-bridged MnCo-hydroxides for flexible high-performance fiber-shaped energy storage device. *Appl. Surf. Sci.* **2019**, 475, 1058-1064.
(21) Naderi, L.; Shahrokhian, S., Nickel molybdate nanorods supported on three-dimensional, porous nickel film coated on copper wire as an advanced binder-free electrode for flexible wire-type asymmetric micro-supercapacitors with enhanced electrochemical performances. *J. Colloid Interface Sci.*, **2019**, 542, 325-338.
(22) Soram, B. S.; Dai, J.; Kshetri, T.; Kim, N. H.; Lee, J. H., Vertically grown and intertwined $Co(OH)_2$ nanosheet@Ni-mesh network for transparent flexible supercapacitor. *Chemical Engineering Journal* **2020**, 391, 123540.
(23) Yu, Y.; Wang, H.; Zhang, H.; Tan, Y.; Wang, Y.; Song, K.; Yang, B.; Yuan, L.; Shen, X.; Hu, X., Blanket-like $Co(OH)_2$/CoOOH/Co_3O_4/$Cu(OH)_2$ composites on Cu foam for hybrid supercapacitor. *Electrochimica Acta* **2020**, 334, 135559.
(24) Zhang, S.; Yin, B.; Wang, Z.; Peter, F., Super long-life all solid-state asymmetric supercapacitor based on NiO nanosheets and alpha-Fe_2O_3 nanorods. *Chem. Eng. J.*, **2016**, 306, 193-203.